

Isospin Dynamics in Sr_2IrO_4 : Forging Links to Cuprate Superconductivity

Jungho Kim,¹ D. Casa,¹ M. H. Upton,¹ T. Gog,¹ Young-June Kim,² J. F. Mitchell,³

M. van Veenendaal,^{1,4} M. Daghofer,⁵ J. van den Brink,⁵ G. Khaliullin,⁶ B. J. Kim³

¹*Advanced Photon Source, Argonne National Laboratory, Argonne, Illinois 60439, USA*

²*Department of Physics, University of Toronto, Toronto, Ontario, Canada M5S 1A7*

³*Material Science Division, Argonne National Laboratory, Argonne, IL 60439, USA*

⁴*Department of Physics, Northern Illinois University, De Kalb, IL 60115, USA*

⁵*Institute for Theoretical Solid State Physics, IFW Dresden,
Helmholtzstr. 20, 01069 Dresden, Germany and*

⁶*Max Planck Institute for Solid State Research, Heisenbergstrae 1, D-70569 Stuttgart, Germany*

(Dated: October 31, 2018)

We used resonant inelastic x-ray scattering to reveal the nature of magnetic interactions in Sr_2IrO_4 , a $5d$ transition-metal oxide with a spin-orbit entangled ground state and $J_{\text{eff}}=1/2$ magnetic moments, referred to as ‘isospins’. The magnon dispersion in Sr_2IrO_4 is well described by an antiferromagnetic Heisenberg model with isospin one-half moments on a square lattice, which renders the low-energy effective physics of Sr_2IrO_4 much akin to that in superconducting cuprates. This is further supported by the observation of excitation modes in Sr_2IrO_4 whose dispersion is strongly renormalized by magnons, which can be understood by analogy to the hole propagation in the background of antiferromagnetically ordered spins in the cuprates.

PACS numbers: 74.10.+v, 75.30.Ds, 78.70.Ck

Quantum magnetism in transition-metal oxides (TMOs) arises from superexchange interactions of spin moments that depend on spin-orbital configurations in the ground and excited states. The array of magnetism in $3d$ TMOs are now well understood within the framework of Goodenough-Kanamori-Anderson [1], which assumes conservation of spin angular momentum in the virtual charge fluctuations. However, it has been recently realized that strong relativistic spin-orbit coupling (SOC) can drastically modify the magnetic interactions and yield far richer spectrum of magnetic systems beyond the standard picture. Such is the case in $5d$ TMOs, in which the energy scale of SOC is on the order of 0.5 eV (as compared to ~ 10 meV in $3d$ TMOs). For example, A_2IrO_3 ($\text{A}=\text{Li}, \text{Na}$) is being discussed as a possible realization of the long-sought Kitaev model with bond-dependent spin interactions [2–4]. Furthermore, strong SOC may result in nontrivial band topology to realize exotic topological states of matter with broken time reversal symmetry, such as a topological Mott insulator [5], Weyl semi-metal and axion insulator [6]. Despite such intriguing proposals abound, the nature of magnetic interactions in systems with strong SOC remains experimentally an open question.

In this Letter, we report on the magnetic interactions in a $5d$ TMO Sr_2IrO_4 with spin-orbit entangled ground state carrying $J_{\text{eff}}=1/2$ moments [7, 8], probed by resonant inelastic x-ray scattering (RIXS). We refer to these $J_{\text{eff}}=1/2$ moments as ‘isospins.’ On theoretical grounds, magnetic interactions of isospins are expected to strongly depend on lattice and bonding geometries. In the particular case of corner sharing oxygen octahedra on a square lattice, relevant to Sr_2IrO_4 [9](Fig. 1(a)), it is predicted that the magnetic interactions of isospins are

described by a pure Heisenberg model, barring Hund’s coupling that contributes a weak dipolar-like anisotropy term [2, 10]. This is surprising considering that strong SOC typically results in anisotropic magnetic couplings that deviate from the pure Heisenberg-like spin interaction in the weak SOC limit. A compelling outcome is that a novel Heisenberg antiferromagnet can be realized in the strong SOC limit, on which a novel platform for high temperature superconductivity (HTSC) may be designed.

RIXS in the last few years has become a powerful tool to study magnetic excitations [11]. We report measurement of single magnons using hard x-rays, which has complementary advantages over soft x-rays as detailed later on. The RIXS measurements were performed using the spectrometer at the 9-1D and the MERIX spectrometer at the 30-ID beamline of the Advanced Photon Source. A horizontal scattering geometry was used with the π incident photon polarization. A spherical diced Si(844) analyzer was used. The overall energy and momentum resolution of the RIXS spectrometer at the Ir L_3 edge (≈ 11.2 keV) was ≈ 130 meV and $\pm 0.032 \text{ \AA}^{-1}$, respectively.

Sr_2IrO_4 has a canted antiferromagnetic (AF) structure [8] with $T_N \approx 240$ K [12], as shown in Fig. 1(b). Although the ‘internal’ structure of a single magnetic moment in Sr_2IrO_4 , composed of orbital and spin, is drastically different from that of pure spins in La_2CuO_4 , a parent insulator for cuprate superconductors, the two compounds share apparently similar magnetic structure. Figures 2(a) and (b) show the dispersion and intensity, respectively, of the single magnon extracted by fitting energy distribution curves shown in Fig. 3(a). We highlight three important observations. First, not only the

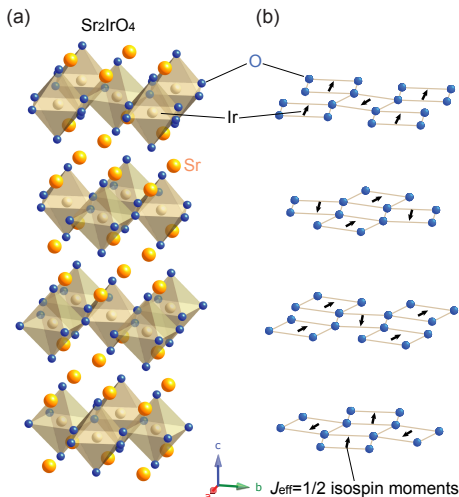


FIG. 1. (a) Due to a staggered in-layer rotation of oxygen octahedra, Sr_2IrO_4 has four IrO_2 layers in the unit cell [9], which coincides with the magnetic unit cell. (b) Isospin one-half ($J_{\text{eff}}=1/2$) moments lie and are canted in the IrO_2 plane [8].

dispersion but also the momentum dependence of the intensity show striking similarities to those observed in the cuprates by inelastic neutron scattering, for instance in La_2CuO_4 [13]. This provides confidence that the observed mode is indeed a single magnon excitation [14–17]. Using hard x-ray RIXS allows mapping of an entire Brillouin zone within only a few degrees of 90° scattering geometry so that the spectrum reveals the intrinsic dynamical structural factor with minimal RIXS matrix element effects. Second, the measured magnon dispersion relation strongly supports the theories predicting that the superexchange interactions of isospins on a square lattice with corner-sharing octahedra are governed by a $\text{SU}(2)$ invariant Hamiltonian with AF coupling [2, 10]. Third, the magnon mode in Sr_2IrO_4 has a bandwidth of ~ 200 meV as compared to ~ 300 meV in La_2CuO_4 [13] and $\text{Sr}_2\text{CuO}_2\text{Cl}_2$ [18], which is consistent with energy scales of hopping t and on-site Coulomb energy U in Sr_2IrO_4 being smaller by roughly 50% than those reported for the cuprates [10, 19, 20].

For a quantitative description, we have fitted the magnon dispersion using a phenomenological J - J' - J'' model [22]. Here, the J , J' , and J'' correspond to the first, second, and third nearest neighbors, respectively. In this model, the downward dispersion along the magnetic Brillouin zone from $(\pi, 0)$ to $(\pi/2, \pi/2)$ is accounted for by a ferromagnetic J' [13, 22]. We find $J=60$, $J'=-20$, and $J''=15$ meV. The nearest neighbor interaction J is again smaller than found in cuprates by roughly 50%. The fit can be improved by including higher order terms from longer-range interactions, which were also found to be important in the case of $\text{Sr}_2\text{CuO}_2\text{Cl}_2$ [18]. However, here we do not pursue this path because, as we show below, another kind of magnetic modes in Sr_2IrO_4 , which is not present in cuprates, may affect the magnon disper-

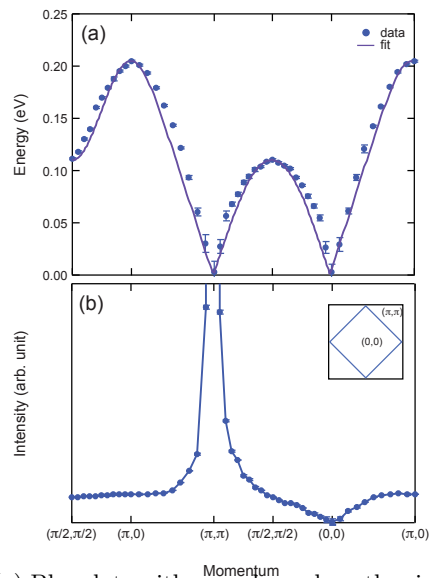


FIG. 2. (a) Blue dots with error bars show the single magnon dispersion extracted by fitting the energy loss curves shown in Fig. 3(b) [21]. The magnons disperse up to ≈ 205 meV at $(\pi, 0)$ and 110 meV at $(\pi/2, \pi/2)$. Solid purple line shows the best fit to the data with $J=60$, $J'=-20$, $J''=15$ meV. (b) Momentum dependence of the intensities showing diverging intensity at (π, π) and vanishing intensity at $(0, 0)$. Inset shows the Brillouin zone of the undistorted tetragonal ($I4/mmm$) unit cell (black square) and the magnetic cell (blue square), and the notation follows the convention for the tetragonal unit cell, as, for instance, in La_2CuO_4 .

sion.

Ultimately, characterizing the magnon mode is important because it strongly renormalizes the dispersion of a doped hole/electron, and is believed to provide a pairing mechanism for HSTC. We now show that Sr_2IrO_4 supports an exciton mode, which gives access to the dynamics of a particle propagating in the background of AF ordered moments even in an undoped case. Figures 3(a) and (b) show the energy loss spectra along high symmetry directions. No corrections to the raw data such as normalization or subtraction of the elastic contaminations have been made. Another virtue of using hard x-ray is that by working in the vicinity of 90° scattering geometry elastic (Thompson) scattering can be strongly suppressed. In addition to low-energy magnon branch (≤ 0.2 eV), we observe high-energy excitations with strong momentum dependence in the energy range of $0.4\sim 0.8$ eV. This mode is superimposed on top of a continuum generated by particle-hole excitations across the Mott gap (estimated to be ≈ 0.4 eV from optical spectroscopy [23]). This is schematically shown in Fig. 3(c). Taking the second derivative of the raw data de-emphasizes the intensity arising from the particle-hole continuum and reveals a clear dispersive feature above 0.4 eV, as shown in Fig. 4(a). The energy scale of this excitation coincides with the known energy scale of spin-orbit coupling in Sr_2IrO_4 ($\zeta_{\text{SO}} \sim 0.5$ eV) [7], and thus

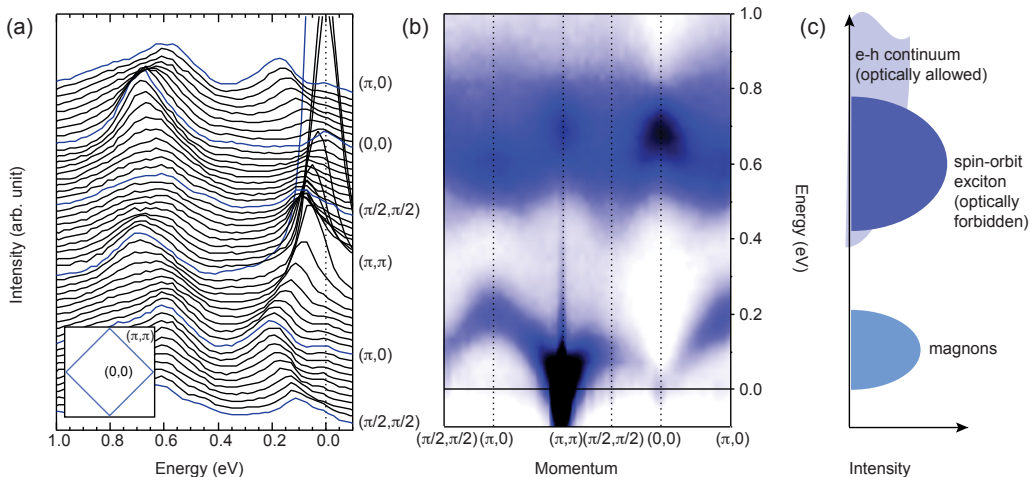


FIG. 3. (a) Energy loss spectra recorded at $T=15$ K, well below the $T_N \approx 240$ K [8, 12], along a path in the constant $L=34$ plane. The path was chosen to avoid the magnetic Bragg peaks, which appear at two of the four corners of the unfolded unit cell (black square) shown in the inset (where the same conventions as in Fig. 2 are used). (b) Image plot of the data shown in (a). (c) Schematic of the three representative features in the data.

we assign it to intra-site excitations of a hole across the spin-orbit split levels in the t_{2g} manifold, i.e. from the $J_{\text{eff}}=1/2$ level to the one of the $J_{\text{eff}}=3/2$ levels [7, 14, 21] (see Fig. 4(c)). We refer to such an excitation as ‘spin-orbit exciton’ [24].

The dispersion of spin-orbit exciton with a bandwidth of at least 0.3 eV implies that this local excitation can propagate coherently through the lattice. Our model of the spin-orbit exciton starts from a recognition that the hopping process is formally analogous to the problem of a hole propagating in the background of AF ordered moments, which has been extensively studied in the context of cuprate HTSC [25]. Although the spin-orbit exciton does not carry a charge, its hopping creates a trail of misaligned spins and thus is subject to the same kind of renormalization by magnons as that experienced by a doped hole [26]. It is well known that the dispersion of a doped hole in cuprates has a minimum at $(\pi/2, \pi/2)$ [27], i.e., at the AF magnetic Brillouin zone boundary. Since Sr_2IrO_4 has a similar magnetic order [8], it can be understood by analogy that the dispersion of the spin-orbit exciton should also have its minimum at $(\pi/2, \pi/2)$.

The overall bandwidth is determined by the parameters involved in the hopping process, which is depicted in Fig. 4(c) in the hole picture. It involves moving an excited hole to a neighboring site, which happens in two steps. First, the excited hole in site i hops to a neighboring site j , generating an intermediate state with energy U' , which is the Coulomb repulsion between two holes at a site in two different spin-orbital quantum levels. Then, the other hole in site j hops back to site i . Thus, the energy scale of the dispersion is set by $2t_{AA}t_{BB}/U'$, which is of the order of the magnetic exchange couplings. In fact, these processes lead to the superexchange interactions responsible for the magnetic ordering, but here they involve both the ground state and excited states of Ir ions.

Technically, the spin-orbit exciton hopping can be described by the following Hamiltonian

$$H = - \sum_{i,j} W_{i,j}^{\alpha\beta} X_{i\alpha}^\dagger X_{j\beta} (b_j^\dagger + b_i), \quad (1)$$

where i indicates the lattice site, b (b^\dagger) is the magnon annihilation (creation) operator, and X denotes the spin-orbit exciton that carries a quantum number α belonging either to the B or C doublet in the $J_{\text{eff}}=3/2$ manifold (see Fig. 3(c)). From this expression, the analogy with the case of a moving hole is apparent; in place of the hopping t for the doped hole, we have an effective spin-orbit hopping matrix W with its overall energy scale set by $W = 2t^2/U$.

We calculated the spin-orbit exciton dispersion by evaluating its self-energy matrix expressed as

$$\Sigma_{\mathbf{k}}^{\alpha\beta} = -z^2 W^2 \sum_{\gamma, \mathbf{q}} \frac{M_{\mathbf{k}, \mathbf{q}}^{\alpha\gamma} M_{\mathbf{k}, \mathbf{q}}^{\gamma\beta}}{\omega_{\mathbf{q}}}, \quad (2)$$

where z is the coordination number and M denotes the vertex [21], using the actual experimental magnon dispersion relation for $\omega_{\mathbf{q}}$ as shown in Fig. 2(a). The only adjustable parameter is W , which only contributes to the overall scaling of the dispersion. The model correctly captures the main features of the data: the locations of extrema in the dispersion (Fig. 4(a)), nearly momentum independent integrated spectral weight (Fig. 4(b)), and the intensity relative to the magnon intensity (Fig. 4(b)). The theory described above is developed in *Supplementary Material*.

Our measurement of the spin-orbit exciton dispersion has important implications in modeling 5d transition-metal oxides with strong SOC. First, it shows that not only the $J_{\text{eff}}=1/2$ states are localized but also the

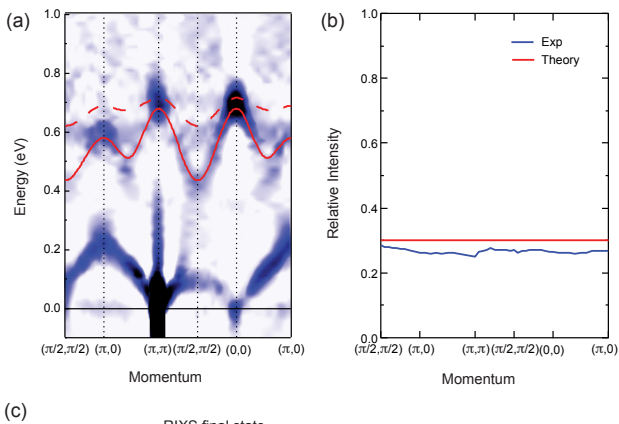


FIG. 4. (a) Second derivative of the data shown in Fig. 3(b), overlaid with the calculation of the dispersion (red solid and dashed lines). The upper branch (dashed line) has less spectral weight than the lower branch (solid line) [21]. $W=63$ meV was chosen in the calculation, which is within the estimated range [21]. (b) Comparison of the experimental and theoretical integrated spectral weight for the two spin-orbit exciton modes normalized to the single magnon mode at $(\pi, 0)$. (c) Schematic of the spin-orbit exciton hopping in the hole representation. By the RIXS process, the hole in the i site is excited to the B/C doublets, which are the $J_{\text{eff}}=3/2$ quartet split by the tetragonal crystal field. This excited hole hops to the neighboring site j with the intermediate energy of U . The other hole in the j site hops back to the i site, thereby completing the spin-orbit exciton hopping processes and also creating a magnon (blue wavy line).

$J_{\text{eff}}=3/2$ states largely retain their atomic-like character. In a contrasting model, in which $J_{\text{eff}}=3/2$ states form an itinerant band and only the $J_{\text{eff}}=1/2$ states are localized, much akin to the orbital-selective Mott transition scenario [28], one expects to see only an electron-hole continuum resulting from the independent propagations of a hole and an electron. Instead, we see the spin-orbit exciton coexisting with the particle-hole continuum; a duality of atomic and band nature of the same $5d$ electrons. Second, the existence of the virtually bound $J_{\text{eff}}=3/2$ states only ~ 0.5 eV above the ground state implies that the superexchange interactions entail multi-orbital contributions. Thus, even for an apparently single orbital $J_{\text{eff}}=1/2$ system such as Sr_2IrO_4 , the magnetic interactions are multi-orbital in character, a fact that must be taken into account in any quantitative model.

Despite such important differences in the high energy scale, our measurement of the magnon spectrum highlights the similarities with cuprates in the low energy effective physics - a rare realization of (iso)spin one-half moments on a square lattice with Heisenberg $\text{SU}(2)$ invariant interactions and comparable magnon bandwidth.

Further, from the observed spin-orbit exciton dispersion, we may expect that a doped hole/electron in Sr_2IrO_4 will display the same dynamics as that observed for a doped hole/electron in the cuprates. The phase diagram of lightly doped Sr_2IrO_4 has just begun to be revealed experimentally [29, 30]. Although superconductivity has not yet been reported, some anomalies that bear strong resemblance to cuprates such as T-linear resistivity have been seen [30, 31]. Only further study will tell if doping can drive Sr_2IrO_4 superconducting.

B. J. K. thanks T. Senthil and H. M. Ronnow for discussions. Work in the Material Science Division and the use of the Advanced Photon Source at the Argonne National Laboratory was supported by the U.S. DOE under Contract No. DE-AC02-06CH11357. Y. K. was supported by the Canada Foundation for Innovation, Ontario Research Fund, and Natural Sciences and Engineering Research Council of Canada. M. vV. was supported by the US Department of Energy (DOE), Office of Basic Energy Sciences, Division of Materials Science and Engineering under Award DE-FG02-03ER46097. This work benefited from the RIXS collaboration supported by the Computational Materials Science Network (CMSN) program of the Division of Materials Science and Engineering, Office of Basic Energy Sciences (BES), US DOE under grant number DE-FG02-08ER46540.

- [1] J. B. Goodenough, *Magnetism and the Chemical Bond* (Interscience, New York, 1963) p. 1329.
- [2] G. Jackeli and G. Khaliullin, *Phys. Rev. Lett.* **102**, 017205 (2009).
- [3] J. Chaloupka, G. Jackeli, and G. Khaliullin, *Phys. Rev. Lett.* **105**, 027204 (2010).
- [4] X. Liu, T. Berlijn, W.-G. Yin, W. Ku, A. Tsvelik, Y.-J. Kim, H. Gretarsson, Y. Singh, P. Gegenwart, and J. P. Hill, *Phys. Rev. B* **83**, 220403 (2011).
- [5] D. Pesin and L. Balents, *Nat. Phys.* **6**, 376 (2010).
- [6] X. Wan, A. Turner, A. Vishwanath, and S. Y. Savrasov, *Phys. Rev. B* **83**, 205101 (2011).
- [7] B. J. Kim, H. Jin, S. J. Moon, J.-Y. Kim, B.-G. Park, C. S. Leem, J. Yu, T. W. Noh, C. Kim, S.-J. Oh, J.-H. Park, V. Durairaj, G. Cao, and E. Rotenberg, *Phys. Rev. Lett.* **101**, 076402 (2008).
- [8] B. J. Kim, H. Ohsumi, T. Komesu, S. Sakai, T. Morita, H. Takagi, and T. Arima, *Science* **323**, 1329 (2009).
- [9] M. K. Crawford, M. A. Subramanian, R. L. Harlow, J. A. Fernandez-Baca, Z. R. Wang, and D. C. Johnston, *Phys. Rev. B* **49**, 9198 (1994).
- [10] F. Wang and T. Senthil, *Phys. Rev. Lett.* **106**, 136402 (2011).
- [11] L. J. P. Ament, M. van Veenendaal, T. P. Devereaux, J. P. Hill, and J. van den Brink, *Rev. Mod. Phys.* **83**, 705 (2011).
- [12] G. Cao, J. Bolivar, S. McCall, J. E. Crow, and R. P. Guertin, *Phys. Rev. B* **57**, R11039 (1998).
- [13] R. Coldea, S. M. Hayden, G. Aeppli, T. G. Perring, C. D. Frost, T. E. Mason, S.-W. Cheong, and Z. Fisk, *Phys.*

- Rev. Lett. **86**, 5377 (2001).
- [14] L. J. P. Ament, G. Khaliullin, and J. van den Brink, Phys. Rev. B **84**, 020403 (2011).
- [15] L. J. P. Ament, G. Ghiringhelli, M. M. Sala, L. Braicovich, and J. van den Brink, Phys. Rev. Lett. **103**, 117003 (2009).
- [16] M. W. Haverkort, Phys. Rev. Lett. **105**, 167404 (2010).
- [17] L. Braicovich, J. van den Brink, V. Bisogni, M. M. Sala, L. J. P. Ament, N. B. Brookes, G. M. D. Luca, M. Saluzzo, T. Schmitt, V. N. Strocov, and G. Ghiringhelli, Phys. Rev. Lett. **104**, 077002 (2010).
- [18] M. Guarise, B. D. Piazza, M. M. Sala, G. Ghiringhelli, L. Braicovich, H. Berger, J. N. Hancock, D. van der Marel, T. Schmitt, V. N. Strocov, L. J. P. Ament, J. van den Brink, P.-H. Lin, P. Xu, H. M. Rønnow, and M. Grioni, Phys. Rev. Lett. **105**, 157006 (2010).
- [19] H. Jin, H. Jeong, T. Ozaki, and J. Yu, Phys. Rev. B **80**, 075112 (2009).
- [20] H. Watanabe, T. Shirakawa, and S. Yunoki, Phys. Rev. Lett. **105**, 216410 (2010).
- [21] See supplementary material for details.
- [22] We do not include the cyclic exchange J_C because magnons cannot distinguish between ferromagnetic J' and J_C . See, for example, Ref. 32.
- [23] S. J. Moon, H. Jin, W. S. Choi, J. S. Lee, S. S. A. Seo, J. Yu, G. Cao, T. W. Noh, and Y. S. Lee, Phys. Rev. B **80**, 195110 (2009).
- [24] T. M. Holden, W. J. L. Buyers, E. C. Svensson, R. A. Cowley, M. T. Hutchings, D. Hukin, and R. W. H. Stevenson, J. Phys. C **4**, 2127 (1971).
- [25] P. A. Lee, N. Nagaosa, and X.-G. Wen, Rev. Mod. Phys. **78**, 17 (2006).
- [26] S. Schmitt-Rink, C. M. Varma, and A. E. Ruckenstein, Phys. Rev. Lett. **60**, 2793 (1988).
- [27] B. O. Wells, Z. X. Shen, A. Matsuura, D. M. King, M. A. Kastner, M. Greven, and R. J. Birgeneau, Phys. Rev. Lett. **80**, 4245 (1998).
- [28] V. I. Anisimov, I. A. Nekrasov, D. E. Kondakov, T. M. Rice, and M. Sigrist, Eur. Phys. J. B **25**, 191 (2002).
- [29] O. B. Korneta, T. Qi, S. Chikara, S. Parkin, L. E. D. Long, P. Schlottmann, and G. Cao, Phys. Rev. B **82**, 115117 (2010).
- [30] M. Ge, T. F. Qi, O. B. Korneta, D. E. De Long, P. Schlottmann, W. P. Crummett, and G. Cao, arXiv:1106.2381v1.
- [31] H. Okabe, N. Takeshita, M. Isobe, E. Takayama-Muromachi, T. Muranaka, and J. Akimitsu, Phys. Rev. B **84**, 115127 (2011).
- [32] A. M. Toader, J. P. Goff, M. Roger, N. Shannon, J. R. Stewart, and M. Enderle, Phys. Rev. Lett. **94**, 197202 (2005).

Supplementary Material: Isospin Dynamics in Sr₂IrO₄: Forging Links to Cuprate Superconductivity

Jungho Kim, D. Casa, M. H. Upton, T. Gog, Young-June Kim, J. F. Mitchell,
M. van Veenendaal, M. Daghofer, J. van den Brink, G. Khaliullin, B. J. Kim

I. RIXS PROCESS AND EFFECTIVE OPERATORS

We describe the RIXS process and derive the effective RIXS operators for the particular case of Sr₂IrO₄^{S1}. The states we use are A_{\pm} for $J_{\text{eff}} = 1/2$ ground state doublet (where the sign takes the role of a isospin degree of freedom) and B_{\pm} and C_{\pm} Kramers doublets for $J_{\text{eff}} = 3/2$ excited states (see Fig. S1). The states A_{\pm} , B_{\pm} , and C_{\pm} depend on spin orbit coupling λ and tetragonal crystal field Δ ^{S2}. The energy splitting Δ between the A_{\pm} states and the B_{\pm}/C_{\pm} subsystem has a dominant contribution from spin-orbit coupling $\frac{3}{2}\lambda$ but also may be contributed by coupling to the lattice; The charge density distribution in the excited $J_{\text{eff}} = 3/2$ states is different from that in the ground state, and hence the orbital flip may cost additional energy. In terms of electron counting, the B and C doublets are completely occupied, while the A level is half filled. We now switch to the hole notation, in which B and C are empty. In the A subsystem, superexchange interactions stabilize an alternating magnetic (isospin) order. We consider the low-energy Hilbert space with singly occupied sites with an empty B/C subsystem, referred to the hole notation. In the Mott insulating ground state, all these levels are coupled by virtual hoppings resulting in a multiorbital superexchange interaction operating within the Hilbert space spanned by $J_{\text{eff}} = 1/2$ and $J_{\text{eff}} = 3/2$ states.

Figure S1 illustrates the RIXS process in the hole representation. The hole in the A level is excited to the $2p$ core levels, also consisting of three doubles (a , b , and c), by absorbing a photon. Subsequently, the excited intermediate state decays back to the t_{2g} manifold, emitting a photon. The excited hole decaying back to the A level with opposite σ corresponds to an effective isospin flip, and the B/C level to an effective spin/orbital flip rela-

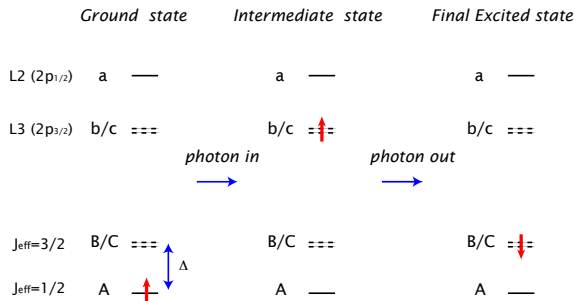


FIG. S1. The RIXS process in the hole representation.

tive to the orbital/spin. To describe the RIXS process mathematically, we define operators X_{σ} , Y_{σ} and Z_{σ} for annihilating a hole in the yz , zx , and xy orbital, respectively. These operators can be expressed in terms of the A_{σ} , B_{σ} , and C_{σ} Kramers doublets as

$$X_{\sigma} = -\frac{\sigma}{\sqrt{2}}(\cos\theta A_{-\sigma} - \sin\theta B_{-\sigma} + C_{-\sigma}), \quad (1)$$

$$Y_{\sigma} = \frac{i}{\sqrt{2}}(\cos\theta A_{-\sigma} - \sin\theta B_{-\sigma} - C_{-\sigma}), \quad (2)$$

$$Z_{\sigma} = \sin\theta A_{\sigma} + \cos\theta B_{\sigma}. \quad (3)$$

Likewise, we define operators for creating a hole in the $2p$ manifold as

$$x_{\sigma} = -\frac{\sigma}{\sqrt{2}}(\cos\phi a_{-\sigma} - \sin\phi b_{-\sigma} + c_{-\sigma}), \quad (4)$$

$$y_{\sigma} = \frac{i}{\sqrt{2}}(\cos\phi a_{-\sigma} - \sin\phi b_{-\sigma} - c_{-\sigma}), \quad (5)$$

$$z_{\sigma} = \sin\phi a_{\sigma} + \cos\phi b_{\sigma}. \quad (6)$$

When the spin-orbit coupling is strong and dominates the crystal field effects, as realized in Sr₂IrO₄^{S3}, then $\cos\phi = \cos\theta = \sqrt{2/3}$.

The effective RIXS amplitude $A_{\mathbf{q}}$ can be defined as

$$A_{\mathbf{q}} \propto \langle f | \sum_{\mathbf{R}} e^{i\mathbf{q}\cdot\mathbf{R}} D^{\dagger}(\epsilon') D(\epsilon) | i \rangle, \quad (7)$$

where D given by

$$D = \sum_{\sigma} (\epsilon_y z^{\dagger} + \epsilon_z y^{\dagger})_{\sigma} X_{\sigma} + (\epsilon_z x^{\dagger} + \epsilon_x z^{\dagger})_{\sigma} Y_{\sigma} + (\epsilon_x y^{\dagger} + \epsilon_y x^{\dagger})_{\sigma} Z_{\sigma} \quad (8)$$

is the dipole transition operator for exciting the valence hole into the p core level, a function of incoming photon polarization ϵ . Likewise D^{\dagger} describes the decay and is a function of the outgoing photon polarization ϵ' .

Integrating out the p manifold and using Eqs.1-3, the effective RIXS operator $\hat{R} \equiv D^{\dagger}(\epsilon') D(\epsilon)$ is obtained. This operator annihilates a particle in the A doublet and creates a particle in the A doublet or in the B/C subsystem:

$$\begin{aligned} \hat{R} &= \sum_{\sigma, \sigma'} \left(\alpha_{\sigma, \sigma'} A_{\sigma'}^{\dagger} + \beta_{\sigma, \sigma'} B_{\sigma'}^{\dagger} + \gamma_{\sigma, \sigma'} C_{\sigma'}^{\dagger} \right) A_{\sigma} \\ &\equiv \hat{R}_A + \hat{R}_B + \hat{R}_C. \end{aligned} \quad (9)$$

The coefficients $\alpha_{\sigma\sigma'}$, $\beta_{\sigma\sigma'}$, and $\gamma_{\sigma\sigma'}$ depend on the scattering geometry and determine the intensities. For the L_2 edge, they all vanish in the limit of cubic symmetry; shown below are the results for the L_3 edge relevant

here. The first term \hat{R}_A describes processes involving the A doublet only and is thus sensitive to magnons. Expressing $A^\dagger A$ in terms of isospin operators, \hat{R}_A can be recast into the form

$$\hat{R}_A = i\frac{2}{3}(P_x S^x + P_y S^y - P_z S^z), \quad (10)$$

where $\mathbf{P} = \epsilon' \times \epsilon$ and \mathbf{S} denotes the isospin within the A doublet. The minus sign in front of the S^z component reflects the fact that the effective g factor of this doublet is opposite to that of real spin because of large orbital moment^{S4}. In principle, the \hat{R}_A can be transformed to a scalar product form, by a simultaneous sign change of the S^x, S^y components.

Performing similar calculations, the matrix elements for the processes described by \hat{R}_B and \hat{R}_C , which create a spin-orbit exciton by promoting a hole from the A states to the B/C levels, can be derived as

$$\beta_{\sigma,\sigma} = \frac{1}{\sqrt{6}}(Q_3 + i\sigma\frac{1}{\sqrt{3}}P_z), \quad (11)$$

$$\beta_{\sigma,-\sigma} = \frac{1}{2\sqrt{2}} \left[\sigma(T_y - \frac{1}{3}P_y) + i(T_x + \frac{1}{3}P_x) \right], \quad (12)$$

$$\gamma_{\sigma,\sigma} = \frac{1}{\sqrt{6}}(Q_2 + i\sigma T_z), \quad (13)$$

$$\gamma_{\sigma,-\sigma} = \frac{1}{2\sqrt{6}} [-\sigma(T_y + P_y) + i(T_x - P_x)], \quad (14)$$

with

$$Q_2 = \epsilon'_y \epsilon_y - \epsilon'_x \epsilon_x, \quad (15)$$

$$Q_3 = \frac{1}{\sqrt{3}}(\vec{\epsilon}' \cdot \vec{\epsilon} - 3\epsilon'_z \epsilon_z), \quad (16)$$

$$T_x = \epsilon'_y \epsilon_z + \epsilon'_z \epsilon_y, \quad (17)$$

$$T_y = \epsilon'_x \epsilon_z + \epsilon'_z \epsilon_x, \quad (18)$$

$$T_z = \epsilon'_y \epsilon_x + \epsilon'_x \epsilon_y. \quad (19)$$

II. MODELING THE SPIN-ORBITON DISPERSION

In a leading approximation (neglecting the intensity transfer between the exciton and magnons due to a mode-mode coupling), the combined spectral weight of $\hat{R}_B + \hat{R}_C$ transitions averaged over the outgoing polarization $\vec{\epsilon}'$ is q -independent, and is given by $\sum_{\sigma,\sigma'} (|\beta_{\sigma,\sigma'}|^2 + |\gamma_{\sigma,\sigma'}|^2) = \frac{2}{9}$. The mode-mode coupling is expected to bring only weak q dependence to the exciton intensity since the related corrections (of the order of J/Δ) are small. This agrees well with the experimental fact that the spectral weight of the high-energy mode is nearly momentum independent.

On the other hand, the magnon intensity which is determined by a dynamical spin structure factor strongly depends on q , see Eq. 10. For the present experimental setup, the RIXS signal is determined by a following

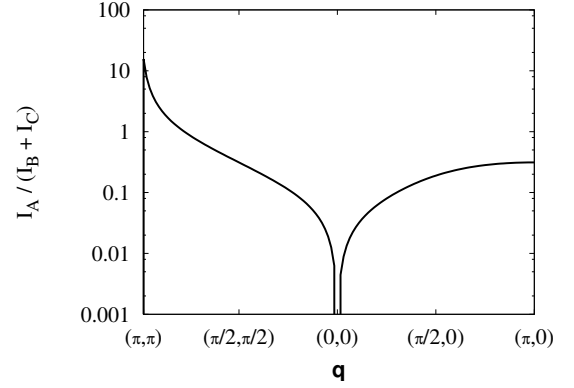


FIG. S2. Spectral weight of the magnon excitation divided by the weight of the excitonic sector at higher energy from the calculation.

combination of the transverse xx, yy and longitudinal zz components of the isospin susceptibility:

$$I_A(\mathbf{q}, \omega) = \frac{1}{9\pi} \left(\frac{3}{2} \chi^{xx} + \chi^{yy} + \frac{3}{2} \chi^{zz} \right)''_{\mathbf{q}, \omega}, \quad (20)$$

from which the intensities of single-magnon $I_A^{(1)}(\mathbf{q})$ and two-magnon $I_A^{(2)}(\mathbf{q})$ processes can be calculated. (In this expression, we neglected weak q dependence of the polarization factors). Within a linear spin-wave theory, we find:

$$I_A^{(1)}(\mathbf{q}) = \frac{1}{9} \frac{5}{8} \sqrt{\frac{A_{\mathbf{q}} - B_{\mathbf{q}}}{A_{\mathbf{q}} + B_{\mathbf{q}}}},$$

$$I_A^{(2)}(\mathbf{q}) = \frac{1}{9} \frac{3}{8} \sum_{\mathbf{k}} \left(\frac{A_{\mathbf{k}} A_{\mathbf{k}+\mathbf{q}} - B_{\mathbf{k}} B_{\mathbf{k}+\mathbf{q}}}{\omega_{\mathbf{k}} \omega_{\mathbf{k}+\mathbf{q}}} - 1 \right), \quad (21)$$

with $A_{\mathbf{q}}, B_{\mathbf{q}}$ and magnon dispersion $\omega_{\mathbf{q}}$ given below in Eqs. 29 and 30.

The relative intensity of the magnon and excitonic modes is a parameter-free result and provides an important test for the consistency of the model and the assignment of the observed modes. The ratio of the intensities of the magnon and the excitonic high-energy modes is shown in Fig. S2. For $q = (\pi, 0)$, for instance, theory predicts the ratio $\simeq 0.3$ which compares well with the experimental value 0.26 of the relative intensities of the low- and high-energy modes. We now discuss the origin of the dispersive features in the excitonic channel. The exciton created by \hat{R}_B and \hat{R}_C delocalizes due to virtual hoppings of electrons as depicted in Fig. 3c. In essence, this propagation is due to a multiorbital superexchange interaction which is responsible for magnetic ordering of the A Kramers doublets, but involving here both the ground $J_{\text{eff}}=1/2$ state and excited $J_{\text{eff}}=3/2$ states of Ir ions. As can be seen in Fig. 3c, the two holes (drawn as isospin arrows) are always in different orbitals. (Virtual processes involving doubly occupied orbitals exist, but do not contribute to exciton delocalization and hence will not be

considered here.) If we neglect the Hund's rule coupling, this implies that the spin of the excited electron plays no role, i.e., the hole-excitation pair can be seen as just a spinless hole, as in the "usual" t - J model derived from the one-band Hubbard model. The hole has, however, an orbital flavor: B or C .

In the two-dimensional space spanned by these two orbitals, the effective hopping matrix for the exciton reads

$$W_{x/y}^{\beta\gamma} = -\frac{2t_{AA}}{U'} \begin{pmatrix} t_{BB} & \pm t_{BC} \\ \pm t_{BC} & t_{CC} \end{pmatrix}, \quad (22)$$

where the inter-orbital element changes sign between the x and y directions. One clearly sees the similarity to the superexchange: the effective exciton hopping is $\propto \frac{t^2}{U'}$, i.e., of the order of J instead of t . [The factor 2 arises because the second step in Fig. 3c can also occur first.]

While the spin of the excited B/C state does not enter the Hamiltonian, the exciton creates a hole in the ordered isospin background of the A system below the magnetic ordering temperature. Following Ref. S5, this hopping connected to magnon creation/annihilation can be written as

$$H_{\text{kin}} = \sum_{i,j,\alpha,\beta} W_{ij}^{\alpha\beta} X_{i\alpha}^\dagger X_{j\beta} (b_j^\dagger + b_i), \quad (23)$$

where we denoted a spin-orbit exciton by $X_{i,\alpha}$. It carries an index i indicating a lattice site and a quantum number α indicating whether it is in the B or C doublets. We see that a hopping of X particle is accompanied by a creation b^\dagger or annihilation b of magnon excitations. $W_{ij}^{\alpha\beta}$ is the orbital- and direction-dependent effective hopping amplitude, see Eq. 22. We consider here only the nearest-neighbor hoppings.

Comparison of our effective Hamiltonian to that of a hole moving in a quantum antiferromagnet reveals that the two problems are equivalent, even though we do not describe a real charge moving at an energy scale of t , but exciton motion with a strongly renormalized hopping matrix $W^{\alpha\beta} = W\tau^{\alpha\beta}$. The energy scale $W = 2t_{AA}^2/U'$ quantifies the exciton hopping amplitude, and Eq. 22 becomes

$$W_{x/y}^{\alpha\beta} = -W \begin{pmatrix} t_{BB}/t_{AA} & \pm t_{BC}/t_{AA} \\ \pm t_{BC}/t_{AA} & t_{CC}/t_{AA} \end{pmatrix} = -W\tau_{x/y}^{\alpha\beta} \quad (24)$$

where $\tau^{\alpha\beta}$ are numbers of the order of one ($t_{BB}/t_{AA} = \frac{5}{4}, t_{BC}/t_{AA} = \pm\frac{\sqrt{3}}{4}, t_{CC}/t_{AA} = \frac{3}{4}$ in the cubic limit used here; the \pm sign depends on x/y bond direction). For nearest-neighbor hopping of the $J_{\text{eff}} = 1/2$ states, $t_{AA} \simeq 0.26$ eV is suggested from band structure calculations^{S6-S8}, and using a representative value of interorbital Coulomb interaction $U' \sim 2$ eV, one estimates $W \simeq 60 - 70$ meV.

Each hopping process creates or destroys magnons. We follow Ref. S5 and treat the AF background in the linear spin-wave theory. After the Bogoliubov transformation, the correlated hopping of exciton (accompanied by

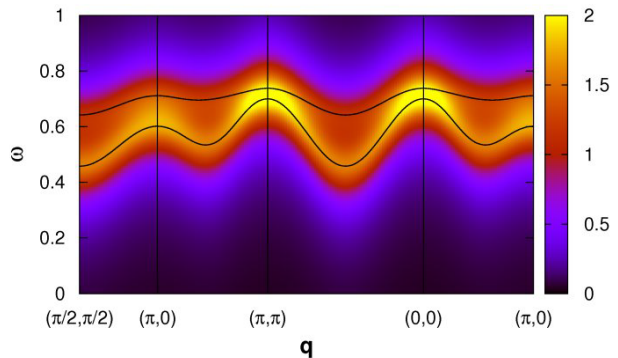


FIG. S3. Dispersion of the hole-excitation pair. Color shading shows the spectrum convoluted with a Lorentzian broadening with width $\delta=100$ meV and weighted with their intensity, see Eq. 32, the lines show the eigenvalues of $\Delta + \Sigma_{\mathbf{k}}$, see Eq. 31. Parameters: $W=63$ meV, $J_1=60$ meV, $J_2=-20$ meV, $J_2=15$ meV, and $\Delta = 0.78$ eV.

a magnon creation/annihilation) reads as follows:

$$H_{\text{kin}} = -zW \sum_{\mathbf{k},\mathbf{q},\alpha,\beta} \left[M_{\mathbf{k},\mathbf{q}}^{\alpha\beta} X_{\alpha\mathbf{k}}^\dagger X_{\beta\mathbf{k}-\mathbf{q}} a_{\mathbf{q}} + h.c. \right]. \quad (25)$$

Except for the orbital index, this is analogous to the t - J model for a doped hole motion in AF-ordered cuprates. Here, $X_{\alpha\mathbf{k}}^\dagger$ ($X_{\alpha\mathbf{k}}$) creates (annihilates) an exciton with momentum \mathbf{k} and orbital flavor α , while $a_{\mathbf{k}}^\dagger$ ($a_{\mathbf{k}}$) creates (annihilates) a magnon, and $z = 4$ is the coordination number. A momentum- and orbital-dependent vertex has been introduced as

$$M_{\mathbf{k},\mathbf{q}}^{\alpha\beta} = |\tau^{\alpha\beta}| (u_{\mathbf{q}} \gamma_{\mathbf{k}-\mathbf{q}}^{\alpha\beta} + v_{\mathbf{q}} \gamma_{\mathbf{k}}^{\alpha\beta}), \quad (26)$$

absorbing the sign change of t_{BC} into the following form-factors:

$$\gamma_{\mathbf{k}}^{\alpha\beta} = \frac{1}{2} \begin{pmatrix} (\cos k_x + \cos k_y) & (\cos k_x - \cos k_y) \\ (\cos k_x - \cos k_y) & (\cos k_x + \cos k_y) \end{pmatrix}. \quad (27)$$

$u_{\mathbf{q}}$ and $v_{\mathbf{q}}$ are Bogoliubov factors and given by the relations

$$u_{\mathbf{q}} = \frac{1}{\sqrt{2}} \sqrt{\frac{A_{\mathbf{q}}}{\omega_{\mathbf{q}}} + 1}, \quad v_{\mathbf{q}} = -\frac{\text{sgn} B_{\mathbf{q}}}{\sqrt{2}} \sqrt{\frac{A_{\mathbf{q}}}{\omega_{\mathbf{q}}} - 1} \quad (28)$$

with

$$A_{\mathbf{q}} = 2(J_1 - J_2 - J_3 + J_2 \cos q_x \cos q_y) + J_3(\cos 2q_x + \cos 2q_y), \\ B_{\mathbf{q}} = J_1(\cos q_x + \cos q_y), \quad (29)$$

and the magnon energy

$$\omega_{\mathbf{q}} = \sqrt{A_{\mathbf{q}}^2 - B_{\mathbf{q}}^2}. \quad (30)$$

The parameters J_1 , J_2 and J_3 denote nearest-neighbor, next-nearest neighbor, and third-neighbor couplings of the isospins \vec{S}_A .

The total Hamiltonian describing the exciton motion in the AF-ordered background contains the kinetic energy H_{kin} as well as the energy of the magnon sector $H_{\text{mag}} = \sum_{\mathbf{q}} \omega_{\mathbf{q}} a_{\mathbf{q}}^{\dagger} a_{\mathbf{q}}$. Since $W_{x/y}^{\alpha\beta}$ is of the order of the J 's rather than the bare hopping t , the present case is slightly different from the ‘‘usual’’ t - J model obtained as a large- U limit of the Hubbard model, where $t \gg J$. The latter describes a strong coupling of holes to magnons, while the present case has a coupling comparable to the magnon energy, $W \sim J$, since both parameters originate from the same multiorbital superexchange interaction. We consequently use perturbation theory to describe the exciton moving in the AF background. Second order perturbation theory leads to an energy correction

$$\Sigma_{\mathbf{k}}^{\alpha\beta} = -(zW)^2 \sum_{\mathbf{q},\gamma} \frac{M_{\mathbf{k},\mathbf{q}}^{\alpha\gamma} M_{\mathbf{k},\mathbf{q}}^{\gamma\beta}}{\omega_{\mathbf{q}}}, \quad (31)$$

with the vertex $M_{\mathbf{k},\mathbf{q}}^{\alpha\beta}$ defined in Eq. 26. This sum can be evaluated numerically, and with parameters $W = 63$ meV and $\Delta = 0.78$ eV we find the dispersive feature shown in Fig. S3.

In Fig. S3, the lines give the two eigenvalues of $\Sigma_{\mathbf{k}}^{\alpha\beta}$, which determine the excitation energies. The weight of the poles can be obtained from the prefactors given in Eq. 11 and the eigenvectors $\cos \theta_{1(2)\mathbf{k}}, \sin \theta_{1(2)\mathbf{k}}$ corresponding to the two eigenvalues of $\Sigma_{\mathbf{k}}^{\alpha\beta}$. The spectral weight of each pole (labeled by 1 and 2) is given by

$$I_{1(2)}(\mathbf{k}) = \sum_{\sigma,\sigma'} [|\beta_{\sigma,\sigma'}|^2 \cos^2 \theta_{1(2)} + |\gamma_{\sigma,\sigma'}|^2 \sin^2 \theta_{1(2)} + \sin \theta_{1(2)} \cos \theta_{1(2)} (\gamma_{\sigma,\sigma'}^* \beta_{\sigma,\sigma'} + \gamma_{\sigma,\sigma'} \beta_{\sigma,\sigma'}^*)]_{\mathbf{k}}. \quad (32)$$

We recall that while the partial intensities $I_1(\mathbf{k})$ and $I_2(\mathbf{k})$ are momentum dependent (via the $\cos \theta_{\mathbf{k}}$ and $\sin \theta_{\mathbf{k}}$ functions) affecting thereby the energy/momentum intensity map, the total spectral weight $I_1 + I_2$ is nearly constant ($= \frac{2}{9}$) over an entire Brillouin zone.

Corrections to the dispersion curves can be calculated within a standard self-consistent Born approximation (SCBA). However, the basic features (such as location of minima at the magnetic Brillouin zone boundary, maxima at Γ and magnetic Bragg points, overall bandwidth of the order of magnon bandwidth, exciton/magnon relative intensities) are expected to remain unchanged since these observations are intrinsic to the model. Based on a well-studied case of hole motion in quantum antiferromagnets, we may expect that the major effect of SCBA calculations will be in a substantial broadening of the exciton lines.

III. EXTRACTION OF THE SINGLE MAGNON DISPERSION

Figure S4 shows the low-energy part of the spectra fit with three peaks along the magnetic Brillouin zone.

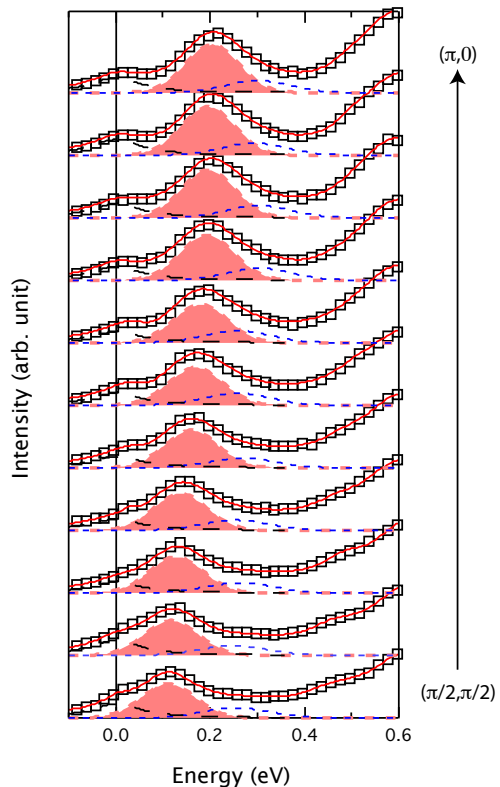


FIG. S4. The single magnon mode extracted from peak fitting. The square markers show the experimental data and the red solid lines shows the fit to the data. The red shaded peak corresponds to the single magnon peak. The dashed black and blue line correspond to the elastic and two magnon peaks, respectively.

The three peaks account for the elastic, single (shaded peaks), and double magnon peaks. The elastic and single magnon peaks were constrained to have a Gaussian width of 130 meV, which is the instrumental resolution determined from the elastic peak at a nonresonant condition. The high-energy modes above ≈ 0.4 eV were also fit with Gaussian functions to account for the tail extending to the magnon modes. The double magnon peaks are not clearly resolved, especially near $(\pi,0)$, which results in some uncertainties in the single magnon peak positions and amplitudes. However, regardless of the fitting procedure used the single magnon peak position was not affected by more than 5 meV.

IV. REFERENCES

- [S1] L. J. P Ament, G. Khaliullin, and J. van den Brink, <http://arxiv.org/abs/1008.4862> (2010).
- [S2] G. Jackeli and G. Khaliullin, Phys. Rev. Lett. **102**, 017205 (2009).
- [S3] B. J. Kim *et al.* Science **323**, 1329 (2009).

- [S4] A. Abragam and B. Bleaney, *Electron Paramagnetic Resonance of Transition Ions* (Clarendon Press, Oxford, 1970).
- [S5] S. Schmitt-Rink, C. Varma, and A. E. Ruckenstein, Phys. Rev. Lett. **60**, 2793 (1988).
- [S6] H. Jin, H. Jeong, T. Ozaki, and Yu, Phys. Rev. B **80**, 075112 (2009).
- [S7] H. Watanabe, T. Shirakawa, and S. Yunoki, Phys. Rev. Lett. **105**, 216410 (2010).
- [S8] F. Wang and T. Senthil, Phys. Rev. Lett. **106**, 136402 (2011).